KAWASAKI STEEL TECHNICAL REPORT
No.32 (March 1995)

Ironmaking Technology, Secondary Refining,
and Center-Segregation Control with Forging in CC

Analysis of Decarburization Reaction in RH Degasser and Its Application to Ultra-low Carbon Steel Production

Yoshiei Kato, Tadasu Kirihara, Tetsuya Fujii

Synopsis :
Theoretical and experimental studies were carried out to quantify the effects of the fluid flow, reaction sites, and geometry of the vacuum vessel on the decarburization characteristics of the RH degasser. The distribution of carbon concentration in the ladle was calculated throughout treatment. The maximum value, found near the bottom of the ladle, was double the minimum value, but this difference was shown to have no effect on the decarburization rate. The ratio of the decarburization rate at the bath surface to the total rate in the RH was greatest in the ultra-low carbon region, while that at the molten steel-refractory interface was the smallest. The maximum decarburization rate and minimum final carbon content between 6 and 12 ppm were attained with the largest vacuum vessel (cross-sectional area, 5.1 m2; inner diameter of snorkel, 1.0 m). On the basis of theoretical and experimental analyses, a procedure was established for determining the geometry of the RH vacuum vessel required to obtain a specified aimed carbon content.

The body can be viewed from the next page.

Analysis of Decarburization Reaction in RH Degasser and Its Application to Ultra-low Carbon Steel Production*

Yoshiei Kato
Dr. Eng., Senior Researcher, Mizushima Ironmaking & Steelmaking Lab., Ironmaking & Steelmaking Res. Dept., Technical Research Labs.

Tadasu Kirihara
Mizushima Ironmaking & Steelmaking Lab., Ironmaking & Steelmaking Res. Dept., Technical Research Labs.

Tetsuya Fujii
Dr. Eng., General Manager, Ironmaking & Steelmaking Res. Dept., Technical Research Labs.

Synopsis:

Theoretical and experimental studies were carried out to quantify the effects of the fluid flow, reaction sites, and geometry of the vacuum vessel on the decarburization characteristics of the RH degasser. The distribution of carbon concentration in the ladle was calculated throughout treatment. The maximum value, found near the bottom of the ladle, was double the minimum value, but this difference was shown to have no effect on the decarburization rate. The ratio of the decarburization rate at the bath surface to the total rate in the RH was greatest in the ultra-low carbon region, while that at the molten steel-refractory interface was the smallest. The maximum decarburization rate and minimum final carbon content between 6 and 12 ppm were attained with the largest vacuum vessel (cross-sectional area, 5.1 m^2; inner diameter of snorkel, 1.0 m). On the basis of theoretical and experimental analyses, a procedure was established for determining the geometry of the RH vacuum vessel required to obtain a specified aimed carbon content.

1 Introduction

The production ratio of ultra-low carbon steel (ULC) as material for interstitial free (IF) steel has increased with recent requirements for improved material-quality features in cold-rolled steel sheet, prompting active development of rapid decarburization technologies for ULC using the RH vacuum degassing equipment (RH) to respond to this trend.[1-5] Proposed methods of enhancing decarburization in the RH include argon injection into the vacuum vassel,[4,5] the use of a higher degree of vacuum in the early stage of decarburization by increasing the evacuation rate,[1,2,4,6] adoption of a higher circulation flow rate of molten steel,[2,4,5] reduction of the amount of molten steel treated,[3] a larger cross-sectional area in the vacuum vessel,[4] and others. However, the fundamental knowledge required to obtain a quantitative grasp of the effectiveness of such measures in increasing the decarburization rate cannot necessarily be called adequate. For example, the existence of a dead zone in the molten steel flow pattern would be related to stagnation in the decarburization process in the ultra-low carbon content region, but study related to the existence of such a dead zone[7-10] has been inadequate and no clear conclusion has been reached. Quantification of the contribution of each reaction site to the decarburization reaction is essential for establishing more effective methods of rapid decarburization, but at present, the reaction sites considered by various researchers differ[2,5,11,12] and no consensus has been obtained. Much research has been done on the effect of RH equipment conditions on the decarburization rate and final carbon content,[2,4,5,13] but because analysis has been limited to the narrow range of currently-existing equipment conditions, a general quantitative understanding of final carbon content and geometry of vacuum vessel has not been achieved.

The effect of these factors on RH decarburization reaction characteristics was therefore clarified through a chemical reaction engineering analysis and experiments, determining the equipment conditions necessary for rapid decarburization with actual equipment.

* Originally published in *Kawasaki Steel Giho*, 25(1993)4, 277-282

2 Effect of Molten Steel Flow on Decarburization Rate

2.1 Theoretical Analysis

2.1.1 Fluid flow in ladle and vacuum vessel

Because molten steel is an incompressible fluid, the fundamental equations is obtained by Eq. (1) and (2).

Equation of continuity:

$$(\nabla \cdot \mathbf{u}) = 0 \quad \cdots\cdots (1)$$

Equation of motion:

$$\rho[\nabla \cdot \mathbf{uu}] = \nabla \cdot (\mu_{\text{eff}} \nabla \mathbf{u}) - \nabla P \quad \cdots\cdots (2)$$

where $\mathbf{u}$: velocity vector of molten steel (m/s)
ρ: density of molten steel (kg/m^3)
P: pressure (Pa)
μ_{eff}: effective viscosity coefficient (kg/m · s)

The value of μ_{eff} is calculated using a κ-ε model, which is a two-equation model for turbulent flow.[14] The numerical calculation was made for a cylindrical coordinate system using the Phoenics general-purpose program. The number of meshes used in calculating the flow in both the ladle and vacuum vessel was 14 for the radial direction, 38 for the cylindrical direction, and 15-38 for the vertical direction.

The molten steel surface in the vacuum vessel shows considerable swelling due to the flow from the up-leg, but it is normally not possible to handle this type of free-surface problem with general-purpose programs such as Phoenics. Repeated calculations corrected by trial and error were therefore made to obtain a surface configuration in which the surface pressure was uniform in all parts.

2.1.2 Decarburization reaction model considering fluid flow

We assumed that the flow of molten steel in the ladle is non-ideal while that in the vacuum vessel is a perfectly mixed flow, and that the decarburization reaction takes place only in the vacuum vessel. If the concept of a residence time distribution function is applied to the carbon balance in the ladle, Eqs. (3)-(5) can be established.

Ladle:

$$C_{\text{out}}(t) = \int_0^\infty C_{\text{in}}(t - t')E(t')\,dt' \quad \cdots\cdots (3)$$

$$C_{\text{L}}(t) = \int_0^\infty C_{\text{in}}(t - t')I(t')\,dt' \quad \cdots\cdots (4)$$

Vacuum vessel:

$$V_{\text{v}} dC_{\text{v}}(t)/dt = Q'\{C_{\text{out}}(t) - C_{\text{in}}(t)\} - akC_{\text{v}}(t) \quad \cdots (5)$$

where $C_{\text{out}}(t)$: carbon content in up-leg (ppm)
$C_{\text{in}}(t)$: carbon content in down-leg (ppm)
$C_{\text{v}}(t)$: average carbon content in vacuum vessel (ppm)
$C_{\text{L}}(t)$: average carbon content in ladle (ppm)
$E(t)$: residence time distribution function (s^{-1})
$I(t)$: internal age distribution function (s^{-1})
V_{v}: volumetric capacity of vacuum vessel (m^3)
Q': circulation flow rate (m^3/s)
ak: capacity coefficient of decarburization reaction (m^3/s)

Although there were no examples of research on $E(t)$ of molten steel in the ladle, Eqs. (6)-(8) were employed using u in the ladle obtained from the fluid calculation described in Sec. 2.1.1, and Eq. (9) was obtained from a numerical analysis of the step response of carbon content at the ladle exit side (up-leg), inputting the carbon content at the ladle inlet (down-leg).[15]

$$\partial C(\mathbf{x}, t)/\partial t = -\mathbf{u} \cdot \nabla C(\mathbf{x}, t) + \nabla \cdot (D_{\text{eff}} \nabla C(\mathbf{x}, t)) \quad \cdots (6)$$

$$t = 0 \quad C_{\text{in}}(t) = C_{\text{out}}(t) = C(\mathbf{x}, t) = 0 \quad \cdots\cdots (7)$$

$$t > 0 \quad C_{\text{in}}(t) = 1.0 \quad \cdots\cdots (8)$$

$$E(t) = dC_{\text{out}}(t)/dt \quad \cdots\cdots (9)$$

$$dI(t)/dt = -E(t) \quad \cdots\cdots (10)$$

$C(\mathbf{x}, t)$: carbon content at point $\mathbf{x}$ in the lade at time t (ppm)
D_{eff}: effective diffusivity (m^2/s)

Accordingly, if Eqs. (3) through (5) are combined and solved, it is possible to calculate the trend in carbon content during RH treatment considering the flow of molten steel in the ladle.

The ladle considered in this calculation had an inner diameter of 4.0 m and bath depth of 3.24 m, for a capacity of 300 t; the up- and down-legs had inner diameters of 0.6 m; and the vacuum vessel had an inner diameter of 2.1 m and bath depth of 0.25 m. The down-leg velocity was 1 m/s, giving the system a circulation flow rate of 120 t/min.

2.2 Results and Discussion

2.2.1 Flow pattern

The calculated flow pattern of the molten steel in the ladle is shown in **Fig. 1**. The fluid emerging from the down-leg shows little tendency to spread and flows along the wall after impinging on the bottom of the ladle. Consequently, a recirculation flow forms at the ladle bottom below the up-leg and to the right of the down-stream. The region affected by fluid suction at the up-leg is limited to the area immediately around the end of the down-leg. The question of whether the recirculation flow constitutes a dead zone is considered in the following section in connection with the trend in the distribution of carbon concentration in the ladle. The calculated results with water and results of a visually observable experiment showed good agreement, although the figures are omitted here. Moreover, the above-mentioned recirculation flow region is observable with other ladle cross-sections, and the two flow paths join in a doughnut shape.[16]

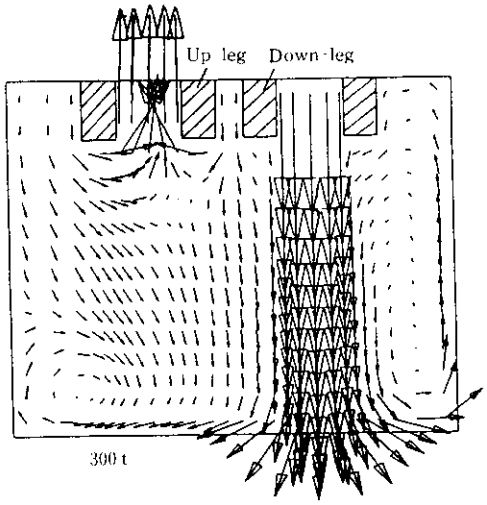

Fig. 1 Calculated flow pattern of steel melt in ladle

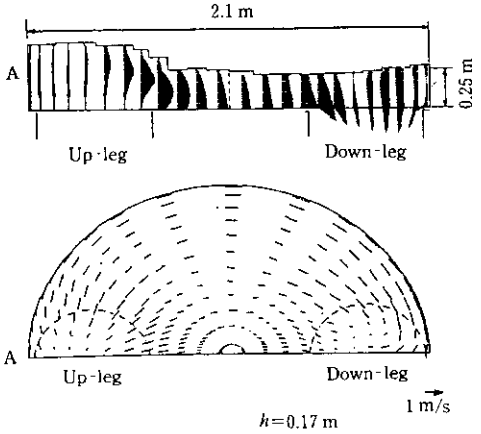

Fig. 2 Calculated flow pattern of steel melt in vacuum vessel

Figure 2 shows the calculated flow pattern of the steel melt in the vacuum vessel. The upper part of the figure is a vertical section joining the center axes between the up-leg and down-leg. The lower part is a plane figure at a height of 0.17 m from the bottom of the vacuum vessel. The figure indicates that the surface of the steel melt above the up-leg is 0.13 m higher than the surface level of a static bath. The flow is smooth between the up-leg and down-leg, and the type of flow which would produce a dead zone does not exist in the vacuum vessel.

2.2.2 Trend of carbon content distribution in ladle

A knowledge of the trend in carbon content at various points in the ladle during decarburization treatment in RH is not only fundamental reaction-engineering material for this process, but is also essential for process improvement and development. However, this

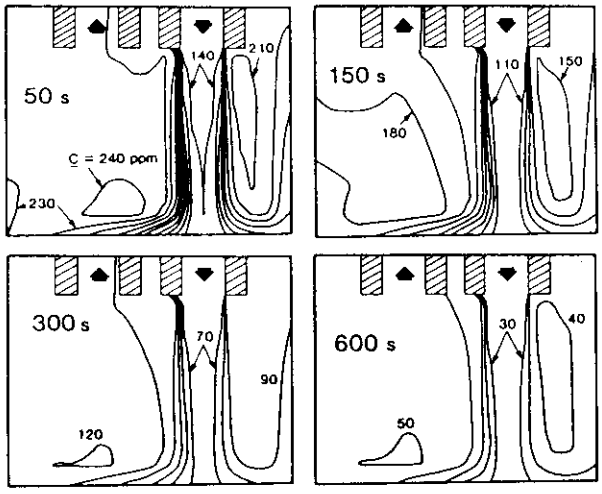

Fig. 3 Contours for carbon content in a vertical section of ladle including center axes of up- and down-legs

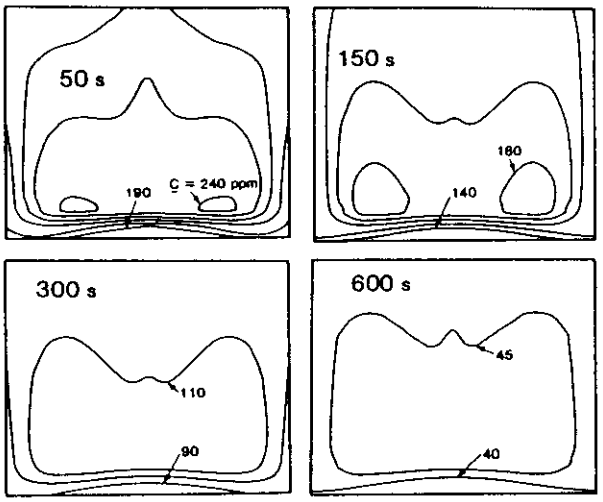

Fig. 4 Contours for carbon content in a vertical section of ladle perpendicular to plane including center axes of up- and down-legs

type of analysis was not performed in the past. Contours of the crbon content at various decarburization periods are shown in **Figs. 3** and **4**. Figure 3 shows vertical sections which include the central axes of the up- and down-legs, while Fig. 4 shows vertical sections perpendicular to the planes shown in Fig. 3. The interval between contour lines represents 5 ppm for a time of 600 s, and 10 ppm in all other cases. Figure 3 shows that at all decarburization periods, the carbon content has its minimum value directly below the down-leg and its maximum value in the recirculation flow region below the up-leg. With time, however, the carbon concentration also decreases in the recirculation flow region shown in Fig. 1, and the maximum carbon content in

the ladle is only about two times the minimum content. Moreover, the decrease in carbon content showed no greatly delayed areas, indicating that no dead zone exists in the ladle. Carbon content showed a high degree of homogeneity in both the vertical section through the up- and down-leg center axes and in the vertical section perpendicular to that plane, although a slightly higher concentration was found in the area of the recirculation flow near the furnace bottom.

The results described above did not locate any area of stagnant decarburization in the ladle which would present an obstacle to decarburization. In the past, it was not possible to finally reject the idea of a dead zone as the reason for stagnation of the decarburization reaction in the final stage of decarburization treatment, but these findings clearly show that the stagnation problem is not attributable to the existence of a dead zone.

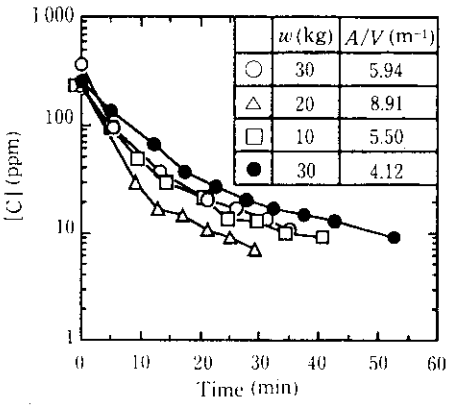

Fig. 5 Influence of amount of molten steel, w, and cross-sectional area of crucible, A, on change of carbon content with time

3 Contribution of Various Reaction Sites to Decarburization Rate

3.1 Experimental Method

A decarburization experiment was performed using a 30-kg vacuum induction furnace in order to clarify the contribution of various reaction sites to the decarburization rate in the low carbon content region under reduced pressure. A magnesia crucible was used. After melting a sample of electrolytic iron with a carbon content of 28 ppm under an argon atmosphere, pig iron was added to adjust the carbon content to an initial level of 200–300 ppm. The experiment then began under conditions of oxygen content, approximately 400 ppm; melt temperature, 1 600°C; and vessel pressure, 133 Pa. As operational factors in the experiment, the amount of molten steel was varied between 10 and 30 kg, and the inner diameter of the crucible at the melt surface; between 0.1 and 0.18 m. Sampling was performed at regular 5 min intervals using a quartz pipe with a diameter of 16 or 8 mm. Carbon analysis was carried out by the combustion method using block samples.

3.2 Experimental Results and Discussion

3.2.1 Effect of various factors on decarburization rate

Figure 5 shows decarburization curves when the amount of molten steel and inner diameter of the crucible at the melt surface were varied, assuming a crucible diameter of 0.18 m and melt weight of 30 kg as basic conditions. **Figure 6** shows the relationship between the carbon content and decarburization rate constant K (min^{-1}). Here, the relationship between K, the interfacial area for reaction, a (m^2), the mass transfer coefficient k (m/min), and the molten steel volume V (m^3) is described by the following equation:

$$K = ak/V \quad \cdots\cdots\cdots\cdots\cdots\cdots\cdots\cdots\cdots\cdots (11)$$

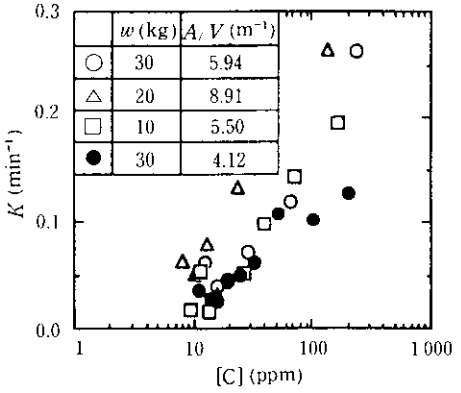

Fig. 6 Relation between rate constant for decarburization and carbon content

In Fig. 5, w represents the amount of molten steel (kg), and A is the cross-sectional area of the crucible (m^2). As can be understood from the plot of circular and triangular symbols in Fig. 5, when the inner diameter of the crucible is held constant and only the amount of molten steel is varied, the decarburization rate is faster when the amount of molten steel is small, at 20 kg. This is because V in Eq. (11) is reduced, even though both a and k are unchanged. In addition, the plots of the circle and square symbols indicate that the diameter of the crucible is changed with the amount of molten steel so that the bath depth remains basically unchanged, but the decarburization rate is substantially the same in the two cases. Again referring to Eq. (11), this is because a/V is substantially the same if the interfacial area for reaction, a, is taken to be the cross-sectional area of the vessel, A. Further, even if the amount of molten steel of 30 kg is taken as a basic condition, the plot of the closed circles, which indicate a 30% reduction in the cross-sectional area of the crucible at the bath surface, shows a lower decarburization rate than under the basic condi-

tion represented by the open circles. This is attributable to a reduction in a in Eq. (11).

To summarize, the decarburization rate increases when the amount of molten steel is decreased or when the surface area of the vessel is increased. However, the effect of the respective reaction sites on the decarburization rate is not clear only from Figs. 5 and 6.

3.2.2 Quantification of contribution of decarburization reaction sites

Assuming that the decarburization reaction progresses at three sites, namely, the free surface of the molten steel bath, the interface between the crucible and the bath, and within the bath, a model of the reaction was created to clarify the respective contribution of each site. The main assumptions of the model are described below.

(1) The mass transfer coefficient is the same at the surface of the bath and at the crucible-bath interface.
(2) The decarburization reaction occurs only at spots where the carbon content is higher than the carbon content C_e, which is in equilibrium with the partial pressure of CO in the ladle.
(3) The driving force $(C - C_e)$ at the crucible-bath interface and in the bath varies with depth h, but as an average value, approximates $(1/2) \times C$.
(4) The reaction area at the free surface of the bath is equivalent to the surface area of the bath, a_A, while that of the crucible-bath interface is in proportion to the area of the lateral face of the crucible, a_S, in the region from the bath surface to a depth h where decarburization can occur from the viewpoint of thermodynamic equilibrium; the interfacial area within the molten steel bath is proportionate to the bath volume $a_A h$.

Using the assumptions described above, the functional relation on ak was obtained by Eq. (12) by the method of least squares from data taken at 18 points in a crucible experiment.

$$ak = 8.5 \times 10^{-5} a_A + 2.0 \times 10^{-5} a_S + 1.3 \times 10^{-3} a_A h \quad \cdots\cdots (12)$$

In Eq. (12), the mass transfer coefficient k is obtained as 8.5×10^{-5} m/s, but Harashima et al. obtained a value of 2.2×10^{-4} m/s, which is larger than that in the present work. The reason for this difference appears to be that the Harashima group gave excessive weight to k because they considered only the free surface of the molten steel as the interfacial area of the reaction.

The relative contribution of each reaction site to the decarburization rate can also be determined from Eq. (12). **Figure 7** shows the relationship between the carbon content and $\{(ak)_i/ak\} \times 100$ in an RH degasser with a vacuum vessel diameter of 2.1 m. The oxygen content was assumed to be 600 ppm. From this figure, the contribution of the reaction site at the refractory-molten steel interface to the decarburization rate was small, at less than 3%, and can be ignored in practical equipment. The greatest contribution to the decarburization rate was made by the inner part of the molten steel bath at C = 18 ppm and over, and below this boundary, by the free molten steel surface. Thus, methods such as Ar injection,[4,5] hydrogen injection[17], and increasing the cross-sectional area of the vacuum vessel,[4,18] the latter being linked to increasing the molten steel surface area, are effective in increasing the interfacial area of the reaction, which should promote the decarburization rate in the ultra-low carbon region.

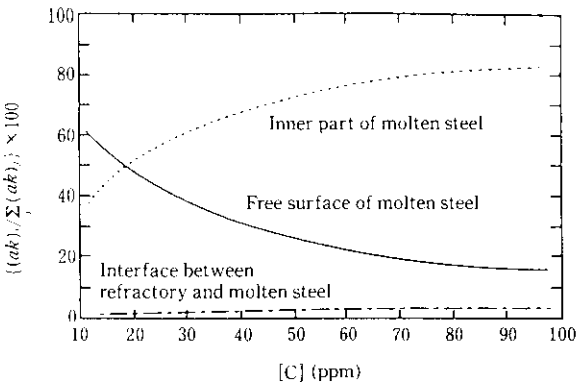

Fig. 7 Effect of each reaction site on decarburization rate during RH treatment

4 Rapid Decarburization Technology with RH Degassers

4.1 Measures to Increase Decarburization Rate and Experimental Conditions

One of the present authors has proposed a decarburization reaction model which assumes that the molten steel in ladle and vacuum vessel comprise a perfectly mixed unit, and proposed the following relationships:[13]

$$C_L = C_L^0 \exp(-Kt) \quad \cdots\cdots (13)$$

$$K = \frac{Q}{W_L}\left(\frac{ak}{Q/420 + ak}\right) \quad \cdots\cdots (14)$$

where C_L^0: initial carbon content in ladle (ppm)
Q: circulation flow rate of steel melt (t/min)
W_L: amount of molten steel in ladle (t)

Equation (14) indicates that the decarburization rate in the RH can be increased by increasing the circulation flow rate or the volumetric coefficient of the decarburization reaction, or by decreasing the amount of molten steel under treatment. The value of Q in Eq. (14) can be estimated using the following equation, which was proposed by Kuwabara et al:[19]

$$Q = 114 G^{1/3} d^{4/3} \{\ln(P_1/P_2)\}^{1/3} \quad \cdots\cdots (15)$$

where G: gas flow rate for circulation of molten steel (Nm^3/min)

Table 1 Design parameters and rate constants for decarburization of RH degasser at Mizushima Works

		No.2 RH			No.4 RH
		Conventional	New vacuum vessel		Conventional
D	(m)	0.6	1.0	0.6	0.75
Q	(t/min)	120	240	90	180
S	(m^2)	3.5	5.1	5.1	4.9
K_{calc}	(min^{-1})	0.18 (Base)	0.30	0.19	0.26
K_{obs}	(min^{-1})	0.18	0.31	0.18	0.24

d: inner diameter of the snorkel (m)

P_1, P_2: respective pressures of atmosphere and in vacuum vessel (Pa)

In Eq. (15), the exponent of d is greater than that of G, indicating that increasing the diameter of the snorkel is more effective than increasing the circulation gas flow rate. Moreover, where the volumetric coefficient of the decarburization reaction is concerned, the decarburization reaction site is proportionate to the cross-sectional area of the vacuum vessel, S (m^2), as is clear from the previous chapter.

$$ak = \alpha S \cdots\cdots (16)$$

Based on the results presented above, a new type of vacuum vessel was designed and fabricated for No. 2 RH at Mizushima Works, aiming at an increased inner diameter of the snorkel (0.6 ⟶ 1.0 m) and increased cross-sectional area of the vacuum vessel (3.5 ⟶ 5.1 m^2). The experimental conditions for No. 2 RH, which were also implemented in parallel at No. 4 RH, are shown in **Table 1**.

4.2 Experimental Results and Discussion

4.2.1 Effect of RH equipment conditions on decarburization rate

Figure 8 shows the trend in carbon content with the conventional vacuum vessel at No. 2 RH, the new vacuum vessel at No. 2 RH, and No. 4 RH. The decarburization rate with the new type of vacuum vessel, in which both the inner diameter of the snorkel and the cross-sectional area of the vacuum vessel were increased ($d = 0.6 \longrightarrow 1.0$ m, $S = 3.5 \longrightarrow 5.1$ m^2), was faster than with the conventional vacuum vessel, and the achieved carbon content was markedly lower, at 6–12 ppm. The decarburization rate with No. 4 RH ($d = 0.75$ m, $S = 4.9$ m^2), which has a circulation flow rate of molten steel and a cross-sectional area of vacuum vessel intermediate between those of the conventional and new type vacuum vessels at No. 2 RH, also falls between

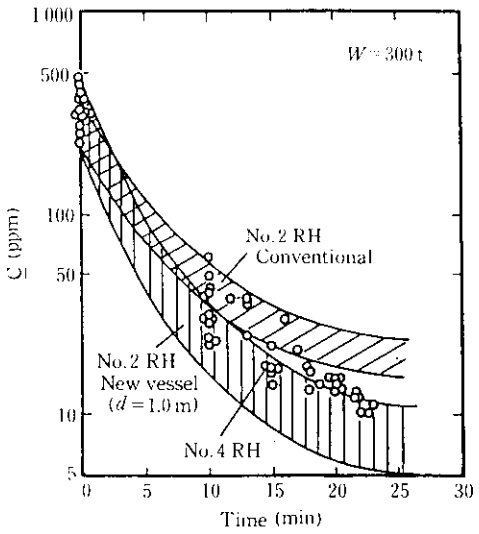

Fig. 8 Change in carbon content in the conventional and new vacuum vessels of No. 2 RH and in the conventinal one of No. 4 RH

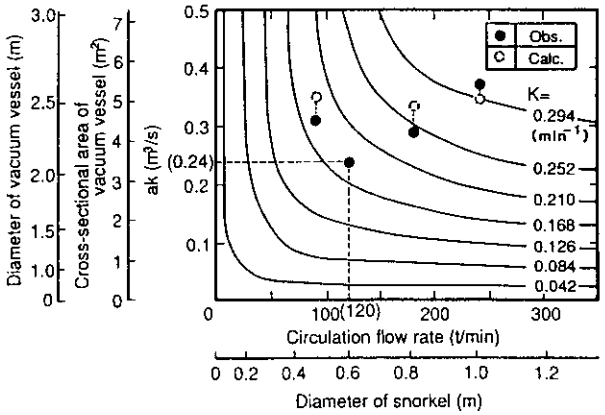

Fig. 9 Relation between capacity coefficient of decarburization and circulating flow rate

those with the two types of vacuum vessels used at No. 2 RH. The achieved carbon content showed the same tendency.

Next, the relationship between the volumetric coefficient of decarburization and the circulation flow rate of molten steel represented by Eq. (14) is shown in **Fig. 9**, with the rate constant of decarburization as a parameter. Based on calculations with Eqs. (15) and (16), values for the cross-sectional area of the vacuum vessel, inner diameter of the vessel, and inner diameter of the snorkel are shown on the axes of the graph. Here, 0.069 was used as the value α in Eq. (16), which is necessary for calculating ak. This value was obtained by inserting into Eqs. (15) and (16) $K = 0.18$ min^{-1}, $Q = 120$ t/min, and $S = 3.5$ m^2 from the conventional vacuum vessel of No. 2 RH. As can be seen in the figure, the

actual and calculated values of K were in good agreement. Figure 9 can thus be used to estimate K for arbitrarily selected RH equipment conditions.

4.2.2 Method of determining geometry of the RH vacuum vessel for aimed carbon content

As discussed above, Fig. 9 provides a useful guideline for increasing the decarburization rate, but because it does not consider the phenomenon of stagnation in decarburization in the ultra-low carbon region, it cannot be used to estimate the final carbon content after the completion of decarburization treatment. If it were possible to estimate final carbon content for all RH equipment conditions, then conversely, it would also be possible to select RH specifications appropriate for an aimed carbon content value. This section will therefore clarify a method for selecting the general RH equipment conditions needed to obtain a target C_f based on the points discussed in the previous section.

Kuwabara et al.[19] and Azuma et al.[5] suggested that the reason for stagnation in the decarburization rate in the ultra-low carbon region is a decrease in the region of the molten steel where decarburization is possible. However, from the viewpoint of thermodynamic equilibrium, the equilibrium carbon concentration can be calculated at 0.8 ppm at $T = 1873$ K, O = 400 ppm, and pressure in the vacuum vessel = 133 Pa (1 Torr). Moreover, as mentioned in the previous chapter, decarburization is possible at the free surface of the molten steel in the RH vacuum vessel, even in what is normally the ultra-low carbon region. Considering these facts, a phenomenon of complete stagnation in the decarburization process is not an adequate explanation. It is also clear from Chapter 2 that stagnation in the decarburization process cannot be attributed to the existence of a dead zone.

In order to describe complete stagnation of decarburization in a numerical expression, the relationship between K and the achieved carbon content C_f was arranged using Eq. (17) as a decarburization rate equation for the ultra-low carbon region.

$$-dC/dt = KC - \beta \cdots\cdots (17)$$

where β is a constant (ppm/min) whose physical meaning is the rate of carbon supply to the molten steel (contamination of the molten steel bath). Decarburization does not occur when $C = C_f$. Therefore, $-dC/dt = 0$, and the following equation can be obtained from Eq. (17):

$$C_f = \beta/K \cdots\cdots (18)$$

Figure 10 shows the relationship between C_f and K for the RH vacuum vessels described in Table 1. C_f is a value after 20–25 min of rimmed treatment. If $C_f = 18$ ppm and $K = 0.18$ min^{-1} for the conventional vacuum vessel of No. 2 RH are substituted into Eq. (18), then $\beta = 3.3$. The figure shows that even if RH conditions

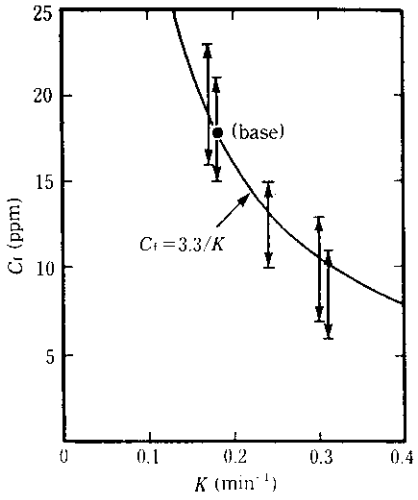

Fig. 10 Relation between final carbon content and rate constant for decarburization

are changed significantly, C_f is inversely proportional to K and decreases as K increases. It can also be understood that the relationship in Eq. (19) obtained from data for the conventional vacuum vessel of No. 2 RH holds for other conditions.

$$C_f = 3.3/K \cdots\cdots (19)$$

Thus, if the rate constant for decarburization in the initial stage can be determined, it is possible to predict the achieved carbon content.

The following is the flow of the method for determining the geometry of the RH vacuum vessel for a target carbon content. After establishing the target value C_f, the value of K is obtained using Eq. (19). Next, the volumetric coefficient of the decarburization reaction and the circulation flow rate are obtained from either Fig. 9 or Eqs. (14) through (16) so as to satisfy the applied value of K, given the dimensions of the ladle and other geometric restrictions. Finally, the diameter of the snorkels, cross-sectional area of the vacuum vessel, and other RH equipment conditions are decided.

5 Conclusions

The effect of molten steel flow and reaction sites on the characteristics of the RH decarburization reaction were clarified by the analysis of chemical reaction engineering and experiments, and the geometry of the RH vacuum vessel necessary for rapid decarburization with actual equipment were proposed.

(1) The flow of molten steel in the ladle was analyzed, and a reaction model was constructed considering the effect of the fluid flow.

(2) The nonuniformity of carbon concentration in the ladle during decarburization treatment has a maximum only approximately two times the minimum,

and the carbon content is steadily reduced even in the recirculation flow region. Accordingly, a dead zone in the RH, which would be an impediment to decarburization, does not exist.

(3) Considering the bath surface, crucible-bath interface, and interior of the bath as reaction sites for the decarburization reaction, an experiment was conducted with a small crucible under reduced pressure to clarify the respective contributions of each site.

(4) According to calculations made under actual RH conditions using an equation for the relationship obtained in the crucible experiment, the contribution of the refractory-molten steel interface to the decarburization reaction is slight at 3% or under. In the ultra-low carbon content region, the contribution of the free surface of the bath is greatest, while in the region of relatively high carbon contents, the contribution of the interior of the bath is greatest.

(5) With a new-type of RH vacuum vessel with the snorkel diameter increased from 0.6 to 1.0 m, the decarburization rate increased significantly and it was possible consistently to obtain final carbon contents of 6-12 ppm.

(6) In the method of deciding the RH equipment conditions needed to obtain a target final carbon content C_f proposed here, the decarburization rate constant K corresponding to C_f is obtained, and the snorkel diameter and cross-sectional area of the vacuum vessel are determined using a relational equation for K obtained from the decarburization model, given the dimensions of the ladle and other geometric restrictions.

References

1) J. Katsuta, T. Saito, H. Mori, H. Tokunaga, M. Takahashi, S. Oyama, and K. Uemura: "Production of ultra low carbon steel," *CAMP-ISIJ,* **3**(1990)1, 152
2) N. Aoki, T. Obana, H. Ikenaga, K. Yoshida, Y. Shirota, and S. Korogi: "Improvement in RH decarburization treatment," *CAMP-ISIJ,* **3**(1990)1, 156
3) Y. Kato, H. Nakato, T. Fujii, S. Ohmiya, S. Suetsugu, M. Suito, and H. Nishikawa: "Development of rapid decarburization technology by combined process of converter and RH degasser for ultra low carbon steel," *CAMP-ISIJ,* **3**(1990)1, 160
4) S. Inoue, T. Usui, Y. Yoshino, and J. Fukumi: "Technology of rapid decarburization treatment in RH process," *CAMP-ISIJ,* **3**(1990)1, 164
5) K. Azuma, S. Onoyama, K. Umezawa, H. Watanabe, K. Ohnuki, and Y. Mizukami: "Investigation of decarburization behavior in RH-reactor and its operation improvement," *CAMP-ISIJ,* **3**(1990)1, 168
6) M. Nadif and D. Brachet: "Production of Ultra Low Carbon Steels at Sollac Dunkirk," 72nd Steelmaking conference, AIME, Chicago (USA), (1989), 227
7) H, Maas: "Principes du procede de degazage de l'acter sous vide par circulation," *Rev. Metall.,* **60**(1963), 421
8) N. Ohtsuki and M. Hattori: "Studies on R-H circulating flow degassing process—On mixing model in ladle," *Fuji-seitsu-Giho,* **16**(1967), 224
9) T. Fujii and I. Muchi: *Tetsu-to-Hagané,* **55**(1969)3, S124
10) S. Korogi, Y. Shirota, and H. Ikenaga: "Decarburization behavior in low carbon content during RH treatment (2)," *CAMP-ISIJ,* **3**(1990)1, 179
11) H. Yetao, T. Sawada, M. Kato, and M. Sano: "Decarburization reaction of molten iron of low carbon concentration with solid oxides," *Tetsu-to-Hagané,* **78**(1992)1, 82
12) K. Harashima, S. Mizoguchi, and H. Kajioka: "Kinetics of decarburization of low carbon liquid iron under reduced pressures," *Tetsu-to-Hagané,* **74**(1988)3, 449
13) N. Sumida, T. Fujii, M. Oguchi, H. Morishita, K. Yoshimura, and F. Sudo: "Production of ultra low carbon steel by combined process of bottom blown converter and RH degasser," *Kawasaki Steel Giho,* **15**(1983)2, 152
14) B. E. Launder and D. B. Spalding: "Mathematical models of turbulence," (1972), [Academic Press]
15) O. Levenspiel: "Chemical reaction engineering (Second edition)," (1972), 263, 291, [John Wiley & Sons, Inc.]
16) Y. Kato, H. Nakato, T. Fujii, S. Ohmiya, and S. Takatori: "Fluid flow in ladle and its effect on decarburization rate in RH degasser," *Tetsu-to-Hagané,* **77**(1991)10, 1664
17) K. Yamaguchi, S. Takeuchi, K. Sorimachi, Y. Kitano, and T. Sakuraya "Hydrogen gas injection for promoting decarburization of ultra low carbon steel in RH degasser", *CAMP-ISIJ,* **61**(1993)1, 177
18) Y. Kato, T. Fujii, S. Suetsugu, S. Ohmiya, and K. Aizawa: "Effect of geometry of vacuum vessel on decarburization rate and final carbon content in RH degasser," *Tetsu-to-Hagané,* **79**(1993)11, 1248
19) T. Kuwabara, K. Umezawa, K. Mori, and H. Watanabe: "Investigation of decarburization behavior in RH-reactor and its operation improvement," *Trans, ISIJ,* **28**(1988), 305